energies

MDPI

Article

Molecular Simulation of Graphene Growth Reactions at Various Temperatures Derived from Benzene in Coal Tar Aromatic Hydrocarbons

Shuhan Zhao, Zhongyang Luo *, Mengxiang Fang, Qinhui Wang and Jianmeng Cen

State Key Laboratory of Clean Energy Utilization, Zhejiang University, Zheda Road 38#, Hangzhou 310027, China; 12227007@zju.edu.cn (S.Z.); mxfang@zju.edu.cn (M.F.); qhwang@zju.edu.cn (Q.W.); jmcen@zju.edu.cn (J.C.)
* Correspondence: zyluo@zju.edu.cn

Abstract: Coal tar, a by-product of the pyrolysis of coal, is rich in aromatic compounds that have the potential to facilitate the synthesis of graphene, a high-quality carbon material, via low-temperature chemical vapor deposition (CVD). This approach offers a promising avenue for the cost-effective and large-scale industrial production of graphene while minimizing energy consumption. Nevertheless, there is a paucity of research focused on the low-temperature synthesis mechanisms of graphene derived from aromatic compounds in the context of graphene growth. To achieve high-quality graphene synthesis from coal tar and its aromatic constituents at reduced temperatures, a comprehensive investigation into the reaction pathways of these aromatic compounds is essential. In this study, we meticulously simulate the pyrolysis of benzene, a key aromatic component of coal tar, across various temperature settings utilizing reactive force field (ReaxFF) methodology. Furthermore, we apply density functional theory (DFT) calculations, executed through the Vienna Ab initio Simulation Package (VASP), to assess the dehydrogenation energy associated with the adsorption of benzene on vapor-deposited copper foils. Our molecular dynamics simulations, enhanced by a mixed force field approach, revealed that the dehydrogenated benzene ring (C_6 intermediate) acts as a critical precursor for graphene synthesis. This research significantly elucidates the reaction pathways of aromatic benzene in coal tar through molecular simulations conducted at different temperatures, both in the gas phase and on solid copper foil substrates.

Keywords: coal tar; aromatic compounds; low energy consumption; graphene; molecular dynamics simulation; ReaxFF; VASP

Academic Editor: Manoj Khandelwal

Received: 30 November 2024
Revised: 12 January 2025
Accepted: 15 January 2025
Published: 17 January 2025

Citation: Zhao, S.; Luo, Z.; Fang, M.; Wang, Q.; Cen, J. Molecular Simulation of Graphene Growth Reactions at Various Temperatures Derived from Benzene in Coal Tar Aromatic Hydrocarbons. *Energies* **2025**, *18*, 392. https://doi.org/10.3390/en18020392

1. Introduction

Coal polygeneration technologies [1] integrate coal pyrolysis and combustion processes, resulting in the production of coal tar and fuel gas within the pyrolysis reactor, as well as steam in the combustion reactor, thereby facilitating power generation and heat supply. These technologies represent a promising approach for the clean and efficient utilization of coal. However, the utilization of tar composition has become a focal point of increasing research interest [2].

Graphene, recognized for its remarkable physical and chemical properties [3], presents substantial opportunities in the fields of electronics [4], energy storage [5], and materials science [6]. Although conventional methods for graphene production, such as mechanical exfoliation [7] and epitaxial growth [8], are capable of producing high-quality graphene, they are inadequate for fulfilling the requirements of large-scale industrial manufacturing.

As a result, there has been considerable research interest in identifying cost-effective and high-yield synthesis methods for graphene. Among them, chemical vapor deposition (CVD) has emerged as a particularly promising technique for the growth of graphene on metallic substrates [9,10], typically employing methane as the carbon source at elevated temperatures exceeding 1000 °C [11]. However, the challenges associated with such high-temperature processes have spurred efforts to develop methods that can achieve graphene synthesis at lower temperatures [12,13]. For example, Sun et al. [14] successfully lowered the temperature for graphene synthesis on copper foil to 750 °C by utilizing C_2H_6 as the carbon source. Similarly, Zhang et al. [15] achieved the production of continuous and large-area monolayer graphene on copper foil at a reduced temperature of 600 °C, employing toluene as the carbon source. Kang et al. [16] synthesized large-scale, low-defect graphene on copper foil at 300 °C under atmospheric pressure, using liquid benzene as the carbon source. Jang et al. [17] produced fully-covered monolayer graphene films on copper foil through an oxygen-free atmospheric pressure chemical vapor deposition (APCVD) process, utilizing benzene as the carbon source at temperatures ranging from 100 °C to 300 °C. Li et al. [18] fabricated graphene films on copper foil surfaces at temperatures between 300 °C and 1000 °C under low pressure, employing solid polymethyl methacrylate (PMMA) and polystyrene (PS) or liquid benzene as carbon sources. Additionally, Choi et al. [19] prepared graphene on copper foil surfaces at a low temperature of 300 °C, utilizing p-terphenyl as the carbon source. Coal tar, abundant in aromatic compounds, presents a promising feedstock for low-temperature graphene synthesis via CVD [20]. In our previous experimental research [20], it was observed that during the process of graphene growth on copper foil surfaces from benzene rings at low temperatures ranging from 300 to 600 °C, the benzene rings did not decompose into small molecular gases but rather deposited on the surface of the copper foil in the form of a six-membered carbon ring. However, based on our experimental research, we could only observe the gas-phase reaction process of the benzene rings. The surface reaction processes of the benzene rings entering the copper foil, including dehydrogenation and graphene migration and nucleation, need to be investigated through simulation calculations. Nevertheless, the intricate chemical reaction pathways and intermediate transformation mechanisms involved remain elusive, hindering its industrial application. Numerous experimental and theoretical investigations have been conducted regarding the growth mechanisms of graphene, with a predominant focus on the chemical vapor deposition (CVD) of graphene utilizing methane-based gaseous carbon sources at elevated temperatures exceeding 1000 °C. It is widely accepted that during the synthesis of graphene from methane, the process of dehydrogenation occurs, resulting in the formation of elemental carbon. This has led to significant efforts in quantum chemical and reaction kinetic simulations aimed at elucidating the transformation of pure carbon atoms into graphene on metallic substrates [21,22]. For example, Meng et al. [23] utilized reactive molecular dynamics to model the growth of graphene from elemental carbon atoms on a Ni(111) surface, identifying an optimal CVD temperature for graphene synthesis at approximately 1000 K, which is consistent with empirical findings. Li et al. [24] conducted a comprehensive analysis of the CVD growth mechanism of graphene from methane at 1300 K, employing a combination of first-principles calculations and efficient kinetic Monte Carlo (KMC) simulations. They posited that the attachment of C_2 species constitutes the primary pathway for graphene growth under these conditions. Collectively, these studies indicate that graphene formation occurs through the decomposition of gaseous precursors, such as methane, on the surface, yielding active species like free carbon atoms or dimers. These active species subsequently organize and coalesce on the surface to establish graphene nucleation centers, which then proliferate into graphene structures. In contrast, Cui et al. [25] employed density functional theory (DFT) calculations to illustrate

that C_5NCl_5 can self-assemble to produce nitrogen-doped graphene. Choi et al. [19] and Tau et al. [26] applied advanced DFT methods to initially explore the CVD preparation mechanism of graphene using liquid and solid carbon sources including benzene, toluene, and p-Terphenyl, which markedly differs from the gaseous carbon source (methane) approach, as the presence of free carbon atoms is minimal during the graphene synthesis process. Tau et al. [27] also studied the growth of graphene on silicon from toluene, which is the most important for practical graphene applications and integration. Lu et al. [28] examined the dynamic deposition process of graphene through molecular dynamics simulations involving naphthalene and fluorene molecules, which deposit and grow graphene on various Ni surfaces at temperatures ranging from 800 to 1100 K. Their findings revealed that naphthalene or fluorene molecules can undergo adsorption, diffusion, and self-assembly reactions on three distinct Ni surfaces to facilitate graphene formation. These investigations suggest that the growth mechanism associated with gaseous carbon sources, exemplified by methane, is not applicable to solid–liquid growth processes represented by aromatic compounds found in coal.

This study aims to unravel the crucial pathways for high-quality, low-energy graphene synthesis through a molecular-level investigation of the pyrolysis of benzene—a fundamental aromatic structure in coal tar—at varying temperatures and its subsequent dehydrogenation and graphene nucleation behavior on copper foil surfaces. Employing reactive force field (ReaxFF) methodology and density functional theory (DFT)-based first-principles simulations using the Vienna Ab initio Simulation Package (VASP, Version 6.3.2), we dissect the pyrolysis products of benzene and their dehydrogenation reactions on copper, validating the hypothesis of dehydrogenated benzene rings (C_6 intermediates) as fundamental building blocks for graphene growth. Our findings aim to pave the way for optimized, energy-efficient graphene production processes from coal tar and provide a theoretical basis for the low-temperature growth of graphene from aromatic compounds such as coal tar.

2. Simulation Tools and Theoretical Methods

2.1. Reactive Force Field (ReaxFF)

ReaxFF is employed for simulating bond formation and bond-breaking processes in organic small molecules, polymeric systems, and reactions such as pyrolysis, combustion, and explosion. Within the ReaxFF model, the interatomic forces or energies are functions of the interatomic distances, which can be calculated using the following expression:

$$E_{system} = E_{bond} + E_{lp} + E_{over} + E_{under} + E_{val} + E_{tor} + E_{vdWaals} + E_{Coulomb}$$

E_{system}—system energy; E_{bond}—bond energy; E_{lp}—long pair electron energy; E_{over}—overcoordination energy penalty; E_{under}—undercoordination stability; E_{val}—valence angle energy; E_{tor}—torsion energy; $E_{vdWaals}$—van der Waals energy; $E_{Coulomb}$—Coulomb energy.

The system energy (E_system) represents the total energy of a system, including the kinetic and potential energies of all particles. Among various components, the long pair electron energy (E_long pair) may refer to the energy associated with long-distance electron pairs in a molecule. Overcoordination leads to an energy penalty (E_overcoordination) due to excess ligands around an atom, while undercoordination can contribute to stability (E_undercoordination) by reducing steric hindrance and charge repulsion. The valence angle energy (E_valence angle) reflects the influence of bond angles on molecular energy, determining its geometry and stability. Torsion energy (E_torsion) arises from the twisting of chemical bonds, affecting molecular conformation and stability. Van der Waals energy (E_van der Waals) represents the weak intermolecular forces due to transient

dipoles, influencing physical properties like solubility and viscosity. Lastly, Coulomb energy (*E*_Coulomb) describes the interaction between charged particles within or between molecules, governed by Coulomb's law.

ReaxFF leverages the bond order–bond distance relationship, coupled with the bond order–bond energy relationship, enabling accurate simulations of chemical bond creation and rupture. All bond–bond connectivity terms, including bond lengths, bond angles, and torsions, are related to bond orders. Non-bonded interactions, comprising van der Waals and Coulombic interactions, do not depend on bond orders but are highly sensitive to the distance between atomic pairs. These interatomic interactions require continuous iterative updates throughout the reaction calculations.

Given our interest in the reactions of benzene in the gas phase at varying temperatures, involving C/H/O atomic species, we adopted the CHO-2016 force field recently developed by Ashraf and van Duin [29]. This force field is capable of simulating the pyrolysis processes of various hydrocarbon fuels, including methane, JP-10, and n-butylbenzene.

Our simulation model consists of randomly packed 100 benzene molecules within a 200 Å × 200 Å × 200 Å cubic space. Using the NVT ensemble, we controlled the simulation temperatures at 800, 900, 1000, 1100, and 1200 K, with a time step of 0.25 fs. The ReaxFF (CHO-2016) model was employed to simulate gas-phase reactions occurring during the growth of graphene from benzene at various temperatures. This approach effectively captures the dynamics of bond breaking and formation, while also elucidating the species and distribution of gas-phase reaction products prior to the interaction of benzene with the copper foil surface.

2.2. Density Functional Theory (DFT) with VASP

DFT, in conjunction with the VASP software (Version 6.3.2) package, was employed to quantify the dehydrogenation energies during the adsorption of benzene on a copper foil surface, exploring the dehydrogenation reaction pathways and directions. VASP, a first-principles-based tool, utilizes density functional theory to solve the Kohn–Sham ground-state energy, incorporating pseudopotential treatments, plane wave basis functions, and periodic boundary conditions. VASP's NEB (Nudged Elastic Band) method accurately computes the energy required to break the C-H bond during the dehydrogenation of a benzene molecule on a copper foil surface as reaction activation energies. Since this process does not involve van der Waals forces, the PBE54 exchange–correlation function was adopted for the calculations.

A (3 × 3) 3-layer unit cell of Cu(111) with 9 copper atoms per layer was selected, with a benzene molecule centered on the surface. A Monkhorst–Pack (1 × 1 × 1) grid was used for Brillouin zone sampling in DFT calculations. During structural optimization, Cu atoms are fixed, while benzene atoms are fully relaxed. A plane wave cutoff energy of 400 eV, an energy convergence criterion of 10^{-5} eV, and a force convergence criterion of 0.02 eV/Å for relaxed structures were employed.

2.3. Hybrid Force Field (Airebo + EAM + LJ)

The released gas was collected in a gas sampling bag attached to the tube furnace exhaust. Prior to pyrolysis, the sampling bags were purged three separate times with hydrogen gas to remove excess air from the sampling bags. The adsorption process of dehydrogenated carbon hexagons on a Cu surface was simulated using a hybrid force field comprising Airebo [30], EAM [31], and LJ [32] potentials.

Airebo Potential: Used for interactions between carbon atoms, Airebo is an empirical many-body potential suitable for simulating the dynamic bond breaking and reforming during deposition growth, particularly for graphene.

EAM Potential: Describes the interactions between copper atoms in the crystal. EAM is a multi-body empirical potential that considers both the interaction potential between atoms in the lattice and the embedding energy of atomic nuclei in the electron cloud.

Lennard–Jones (LJ) Potential: Models the interactions between carbon atoms in graphene and copper atoms. LJ is a pairwise interaction model for neutral atoms or molecules.

The copper substrate model comprises 3 layers of copper atoms with dimensions of 37 Å × 20 Å × 37 Å. The (111) surface of the copper crystal was chosen for adsorption simulations, with periodic boundary conditions applied to the model boundaries. To enhance computational efficiency, a simplified model using cracked six-membered carbon rings as the carbon source was adopted. The simulation temperature was controlled within a temperature range of 500–1300 K, with a time step of 0.001 ps.

3. Results and Discussion

3.1. Study on the Gas-Phase Reaction of Benzene at Low Temperature upon Entering the Copper Foil Surface

The growth behavior of graphene films on copper foil surfaces can be delineated into three distinct stages: pyrolysis of the carbon source, nucleation of graphene, and the growth of graphene. Initially, when the carbon source is introduced into the chemical vapor deposition (CVD) system, it undergoes a gas-phase reaction, specifically pyrolysis, which results in the formation of active carbon species prior to their deposition on the copper foil surface. These active carbon species then experience further dehydrogenation and pyrolysis on the substrate, leading to the establishment of the fundamental carbon structure of graphene. Through processes of migration and aggregation, carbon clusters are generated, which subsequently capture additional active carbon species from the surrounding environment, thereby facilitating the formation of stable graphene nuclei. Ultimately, active carbon species persistently migrate to the growth fronts of the graphene domains on the substrate surface, continuously supplying the necessary raw materials for the growth and development of graphene films.

However, the gas-phase reaction laws for graphene growth vary significantly with different carbon sources and temperatures. For methane, a commonly used carbon source for graphene CVD growth, the gas-phase reactions typically occur at temperatures above 1000 °C, where methane forms various active carbon species such as C_2H_4, C_2H_6, C_2H_3, C_3H_3, C_3H_6, C_6H_5, and C_6H_6 [33]. In contrast, benzene, as a unique carbon source capable of growing graphene at low temperatures (100–900 K), has been experimentally demonstrated to enter the copper foil surface as intact benzene rings without undergoing ring-opening pyrolysis within the temperature range of 300–600 °C (573–973 K). Through the analysis of 100 molecular dynamics simulations of benzene utilizing the ReaxFF force field, conducted over a consistent simulation duration of 12.5 ns (as detailed in Table 1), it was observed that benzene molecules do not exhibit ring-opening pyrolysis at temperatures below 1000 K. However, within the temperature range of 1000 K to 1200 K, partial cracking of benzene molecules occurs, leading to the formation of various active carbon species. Furthermore, it was noted that the quantity of cracked benzene rings escalates with increasing temperatures, resulting in a more varied and intricate array of active carbon species.

Consequently, within the temperature parameters established for the synthesis of graphene utilizing benzene, the low-temperature conditions prevent the occurrence of gas-phase pyrolysis of benzene. This enables the intact benzene rings to penetrate the surface of the copper foil, facilitating subsequent dehydrogenation, which will be elaborated upon in the following discussion.

Table 1. Molecular dynamics simulation of vapor-phase reaction product distribution for the incorporation of benzene rings as carbon sources into copper foil for graphene growth.

Temp/K	800	900	1000	1100	1200
C6	100	100	96	84	80
C					3
C2			1	4	9
C3					1
C4			1		
C5				1	1
C6				6	2
C7				1	7
C8			1	1	1
C9					
C10			1		
C11					
C12				2	1

3.2. Dehydrogenation Process of Benzene Rings on the Copper Foil Surface

As discussed in the previous section, intact benzene rings undergo dehydrogenation upon entering the copper foil surface. The energy change during the dehydrogenation reaction is illustrated in Figure 1. Based on molecular dynamics simulations of a 3 × 3 × 3 copper foil surface, the dehydrogenation order of benzene rings on the copper surface is 1→2→3→4. The dehydrogenation process involves stretching the distance between C and H atoms (originally 1.1 Å in the benzene ring) to three times its original length (3.3 Å). Using the image nudged elastic band (NEB) method to calculate the energy changes during the dehydrogenation process of benzene rings adsorbed on the surface of copper foil, we found that the energy barrier for the first hydrogen detachment from the benzene ring on copper foil is 0.89 eV. It should be clarified that the dehydrogenation energy we have calculated (0.89 eV) pertains to the energy barrier required to break the carbon–hydrogen bond of a benzene ring on the surface of copper foil during its dehydrogenation process. This value differs from the dehydrogenation energy (1.67 eV) reported by Tau et al. [26], which they calculated for the process of benzene adsorption on copper foil.

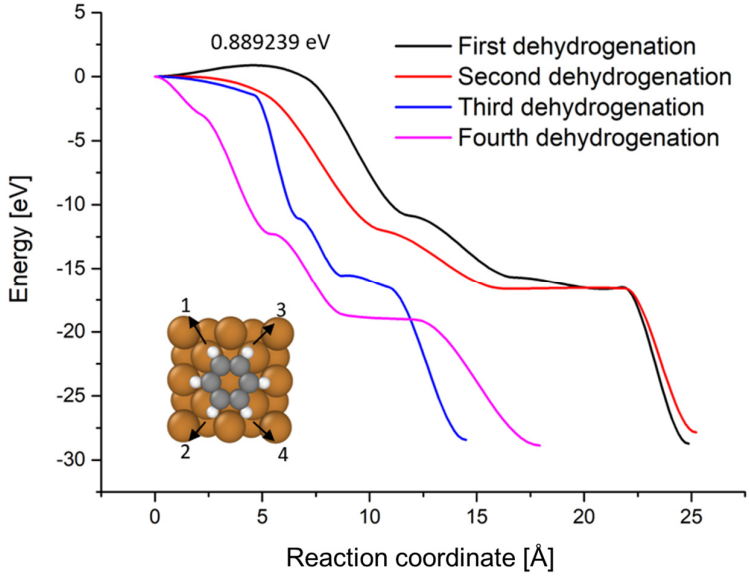

Figure 1. Energy changes and the sequence of dehydrogenation for the first four hydrogen atoms of benzene on the surface of copper foil.

Subsequent detachments of hydrogen atoms 2–6 from the benzene ring on the copper surface do not necessitate overcoming additional energy barriers. Notably, the detachment of the fifth and sixth hydrogen atoms is accompanied by an energy increase but does not exceed the energy of the original structure (Figure 2). This indicates that once the energy barrier of 0.89 eV for the first hydrogen detachment is overcome, the subsequent detachment of the other five hydrogen atoms is facile, leading to the formation of a six-membered carbon ring structure on the copper foil surface.

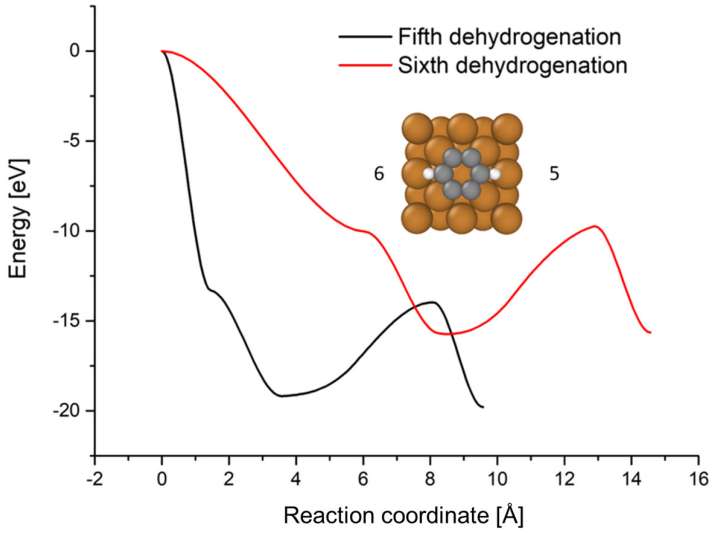

Figure 2. Energy changes and the sequence of dehydrogenation for the last two hydrogen atoms of benzene on the surface of copper foil.

The energy level changes during the dehydrogenation process of a benzene ring on a copper foil surface, as illustrated in Figure 3, show that the overall dehydrogenation process is characterized by a continuous decrease in energy. Except for the initial dehydrogenation step, which requires a small energy barrier, the energy barriers for the subsequent dehydrogenation reactions are nearly zero. Additionally, the energy values for these dehydrogenation reactions are not identical, although they exhibit similar trends in change.

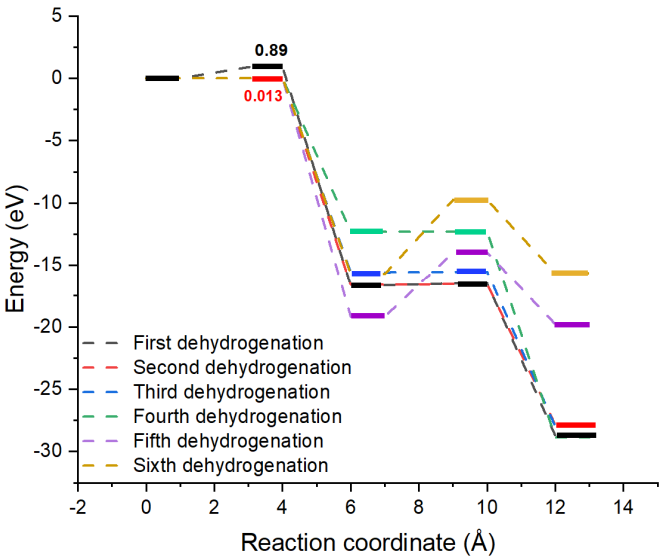

Figure 3. Energy level diagram for the dehydrogenation of the benzene ring on the copper foil surface (loss of six hydrogen atoms).

The bond energy of the carbon–hydrogen bond within the benzene ring, measured at 3.9 eV, is considerably higher than the energy necessary, 0.89 eV, for the dehydrogenation on copper foil. This indicates that copper foil plays a substantial catalytic role in the dehydrogenation process of benzene. Consequently, this phenomenon elucidates the feasibility of synthesizing graphene on copper foil utilizing benzene as a carbon precursor at reduced temperatures. The rate of dehydrogenation is determined through the application of the Arrhenius equation [19]:

$$R(T) = Aexp(-\frac{E_a}{K_B T}),\ A = \frac{K_B T}{h}$$

where A is the pre-exponential factor, E_a is the activation energy, R is the gas constant, T is the temperature, and h is Planck's constant.

Based on the calculated rates, the required time for the dehydrogenation of benzene rings at different temperatures is presented in Table 2 below.

Table 2. Time for the dehydrogenation of benzene rings at different temperatures.

Temperature for Graphene Growth/K	Time */s
300	129.26
400	0.018
500	8.4×10^{-5}

* $time = \frac{1}{R(T)}$.

At a temperature of 300 K (room temperature), the duration of dehydrogenation is significantly prolonged, as indicated in Table 2, with a time of 129.26 s, and the reaction is virtually negligible. Conversely, when the temperature is elevated to 400 K, the reaction time decreases dramatically to 0.018 s, facilitating the onset of dehydrogenation and resulting in the formation of graphene on the surface of the copper foil. Our findings are consistent with experimental data, demonstrating that graphene can be synthesized from benzene at 100 °C (273 K), whereas such synthesis does not occur under identical reaction conditions at room temperature [17].

In summary, during the chemical vapor deposition process for graphene growth, the benzene on the surface of copper foil first undergoes dehydrogenation in a specific sequence to remove all hydrogen atoms, and then serves as the basic feedstock unit for graphene synthesis in the form of six-membered carbon rings.

3.3. Splicing Growth of Graphene from Basic Building Blocks: Six-Membered Carbon Rings

Molecular dynamics simulations using a hybrid force field (Airebo + EAM + LJ) were conducted to investigate the splicing behavior of six-membered carbon rings (6 × 6) formed by dehydrogenation on the copper foil surface at various temperatures, as shown in Figure 4.

At 500 K, the six-membered carbon rings undergo complete splicing to form multiple graphene domains, although these domains are relatively dispersed. The schematic diagram (Figure 5a) illustrates the method by which carbon six-membered rings are assembled to form graphene. The specific splicing mode involves head-to-head connections of two carbon rings, with the third ring contributing two carbon atoms for compensation. At this temperature, graphene defects primarily manifest as holes formed by the connections of the multiple six-membered carbon rings shown. As shown in Figure 5c, these cavities may be formed by the side-by-side arrangement of three-, four-, five-, or even more six-membered carbon rings [34]. We can name these cavities defects generated during the growth of a six-membered carbon ring first-type defects. Within the temperature range of 600–1000 K,

graphene domains begin to coalesce, accompanied by the emergence of eight-membered ring defects. These defects arise from the cracking of one ring during the pairwise splicing of six-membered rings (Figure 5b). The eight-membered ring defects produced by ring opening can be named second-type defects.

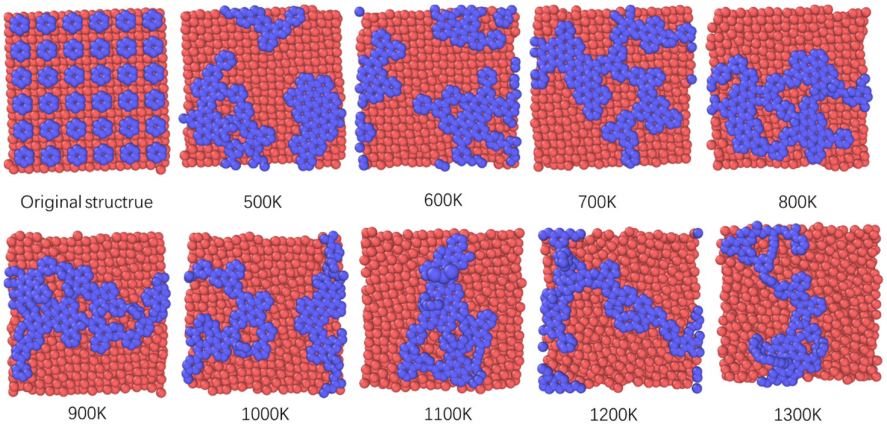

Figure 4. Molecular dynamics simulation of the migration of six-membered carbon rings on the surface of copper foil for the synthesis of graphene.

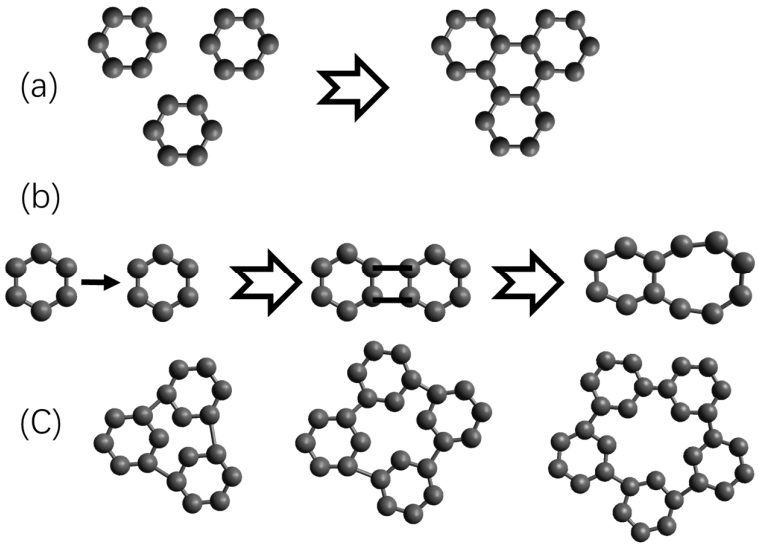

Figure 5. Assembly of graphene from six-membered carbon rings and their assembly defects. (**a**) Synthesis of Graphene from Six-Membered Carbon Rings (**b**) second-type defect (**c**) first-type defects.

As the reaction temperature increases, certain graphene structures begin to display three-dimensional defects, characterized by one end being elevated. At temperatures exceeding 1100 K, while the concentration of graphene domains intensifies, the six-membered carbon rings on the copper foil surface start to open actively, resulting in the formation of larger defects. At 1200 K and 1300 K, it becomes increasingly challenging to observe intact graphene structures during the splicing process. Figure 6 illustrates the distribution of various defect types encountered during the synthesis of graphene from six-membered carbon rings at different temperatures.

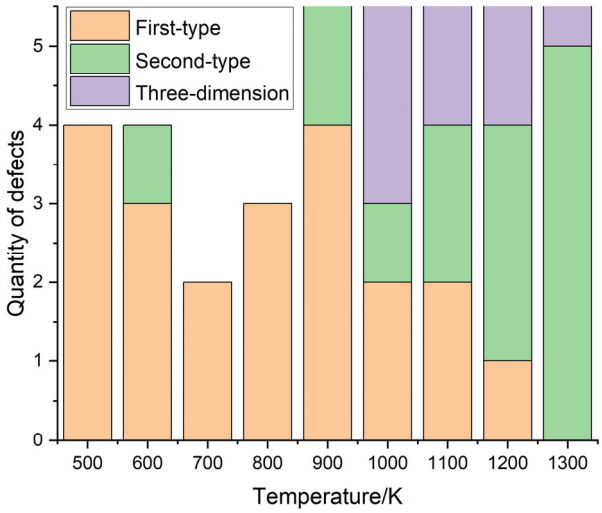

Figure 6. The quantity and types of defects within six-membered carbon ring graphene structures at varying temperatures.

In general, at lower synthesis temperatures ranging from 500 K to 800 K, the first type of defect predominates. In the temperature range of 900 K to 1300 K, an increase in temperature correlates with a gradual rise in the second type of defect, while the first type of defect diminishes. Above 1200 K, graphene is primarily characterized by the second type of defect, with the first type nearly absent. Three-dimensional defects begin to emerge around 1000 K but tend to decrease as the temperature continues to rise.

Regardless of whether the temperature is in the high or low range, the minimum temperature for synthesizing graphene with minimal defects is established at 700 K. This finding suggests that six-membered carbon rings derived from benzene can act as fundamental units for graphene growth through direct migration and splicing at temperatures below 1000 K. However, elevated temperatures result in an increase in both the variety and quantity of defects within the graphene structure. These results underscore the significant influence of temperature on the synthesis of graphene using benzene as a carbon source, thereby highlighting the necessity of selecting an appropriate temperature range to enhance the quality of the graphene produced.

4. Conclusions

In this study, we conducted a systematic investigation into the vapor-phase reaction of benzene, utilized as a carbon source on copper foil surfaces at low temperatures, specifically within the range of 100 K to 900 K, and examined the associated mechanisms of graphene growth. By integrating theoretical simulations with experimental validation, we identify distinct pathways and critical factors that influence the growth of graphene from benzene on copper foil.

Initially, we elucidate the characteristics of the vapor-phase reaction of benzene on copper foil surfaces under low-temperature conditions (below 1000 K). Unlike carbon sources such as methane, which undergo transformations at elevated temperatures, benzene predominantly retains its ring structure within this temperature range, thereby avoiding ring-opening cleavage and engaging in subsequent reactions as intact benzene rings. This finding presents novel options for carbon sources and enhances our understanding of graphene growth pathways at low temperatures.

Subsequently, we explored the dehydrogenation process of benzene rings on copper foil surfaces. Our simulations indicate that the initial detachment of a hydrogen atom from the benzene ring on copper foil necessitates overcoming an energy barrier of 0.89 eV,

while the removal of subsequent hydrogen atoms occurs with relative ease. The copper foil demonstrates a pronounced catalytic effect on the dehydrogenation of benzene rings, significantly lowering the energy requirements for this reaction. Calculations employing the Arrhenius equation reveal that the dehydrogenation of benzene rings and the nucleation of graphene can occur at an unexpectedly low temperature of 400 K (100 °C).

Furthermore, we investigated the direct stitching growth mechanism of six-membered carbon rings, which are formed through the dehydrogenation of benzene rings on copper foil surfaces. Within the temperature range of 500 K to 1000 K, six-membered carbon rings can exist stably and contribute to the formation of graphene domains through migration and stitching, exhibiting a minimal number of hole defects (two defects) at 700 K. However, as temperatures increase to between 1000 K and 1300 K, the growth of graphene begins to display structural defects, including eight-membered rings and three-dimensional warping. This indicates that while higher temperatures promote domain agglomeration, they also elevate the defect density within the graphene structure. Consequently, the selection of an appropriate temperature range is essential for optimizing the quality of graphene growth.

In conclusion, this study elucidates the unique pathway for graphene growth from benzene as a low-temperature carbon source on copper foil. Benzene rings synthesize graphene through dehydrogenation on copper foil, forming graphene as a basic unit of six-membered carbon rings. These findings not only provide a theoretical basis for the low-temperature growth of graphene from aromatic compounds such as coal tar pitch but also offer new strategies and theoretical foundations for the efficient and high-quality growth of graphene under low-temperature conditions. Potentially, this could advance the application and development of graphene materials across various fields. Future research may further investigate the catalytic effects of different metal substrates on benzene dehydrogenation and graphene growth, as well as optimize growth conditions to enhance graphene performance and yield.

Author Contributions: S.Z., conceptualization, methodology, writing—original draft preparation, visualization, investigation, and modeling and simulation. Z.L. and M.F., results interpretation and writing—reviewing and editing. Q.W. and J.C., supervision and funding acquisition. All authors have read and agreed to the published version of the manuscript.

Funding: This work was supported by the Fundamental Research Funds for the Central Universities (2022ZFJH004).

Institutional Review Board Statement: Not applicable.

Informed Consent Statement: Not applicable.

Data Availability Statement: All of the data have been included in the text.

Acknowledgments: The authors extend their appreciation to the Fundamental Research Funds for the Central Universities (2022ZFJH004) and State Key Laboratory of Clean Energy Utilization in Zhejiang University.

Conflicts of Interest: The authors declare no conflicts of interest.

References

1. Yu, P.; Luo, Z.; Wang, Q. Life cycle assessment of transformation from a sub-critical power plant into a polygeneration plant. *Energy Convers. Manag.* **2019**, *198*, 111801. [CrossRef]
2. Ma, Z.; Wei, X.; Liu, G. Value-added utilization of high-temperature coal tar: A review. *Fuel* **2021**, *292*, 119954. [CrossRef]
3. Geim, A.K.; Novoselov, K.S. The rise of graphene. *Nat. Mater.* **2007**, *6*, 183–191. [CrossRef] [PubMed]
4. Castro Neto, A.H.; Guinea, F.; Peres, N.M.R. The electronic properties of graphene. *Rev. Mod. Phys.* **2009**, *81*, 109–162. [CrossRef]
5. Liu, C.; Yu, Z.; Neff, D. Graphene-based supercapacitor with an ultrahigh energy density. *Nano Lett.* **2010**, *10*, 4863–4868. [CrossRef] [PubMed]

6. Bunch, J.S.; Verbridge, S.S.; Alden, J.S. Impermeable atomic membranes from graphene sheets. *Nano Lett.* **2008**, *8*, 2458–2462. [CrossRef]
7. Novoselov, K.S.; Geim, A.K.; Morozov, S.V. Electric field effect in atomically thin carbon films. *Science* **2004**, *306*, 666–669. [CrossRef]
8. Emtsev, K.V.; Bostwick, A.; Horn, K. Towards wafer-size graphene layers by atmospheric pressure graphitization of silicon carbide. *Nat. Mater.* **2009**, *8*, 203–207. [CrossRef]
9. Ruan, G.; Sun, Z.; Peng, Z. Growth of graphene from food, insects, and waste. *ACS Nano* **2011**, *5*, 7601–7607. [CrossRef]
10. Sharma, S.; Kalita, G.; Hirano, R. Synthesis of graphene crystals from solid waste plastic by chemical vapor deposition. *Carbon* **2014**, *72*, 66–73. [CrossRef]
11. Li, X.; Cai, W.; An, J.; Kim, S.; Nah, J.; Yang, D.; Piner, R.; Velamakanni, A.; Jung, I.; Tutuc, E. Large-Area Synthesis of High-Quality and Uniform Graphene Films on Copper Foils. *Science* **2009**, *324*, 1312–1314. [CrossRef] [PubMed]
12. Muñoz, R.; Gómez-Aleixandre, C. Review of CVD synthesis of graphene. *Chem. Vap. Depos.* **2013**, *19*, 297–322. [CrossRef]
13. Kim, B.J.; Nasir, T.; Choi, J.-Y. Direct growth of graphene at low temperature for future device applications. *J. Korean Ceram. Soc.* **2018**, *55*, 203–223. [CrossRef]
14. Sun, X.; Lin, L.; Sun, L. Low-Temperature and Rapid Growth of Large Single-Crystalline Graphene with Ethane. *Small* **2018**, *14*, 1702916. [CrossRef]
15. Zhang, B.; Lee, W.H.; Piner, R. Low-temperature chemical vapor deposition growth of graphene from toluene on electropolished copper foils. *ACS Nano* **2012**, *6*, 2471–2476. [CrossRef]
16. Kang, C.; Jung, D.H.; Lee, J.S. Atmospheric Pressure Chemical Vapor Deposition of Graphene Using a Liquid Benzene Precursor. *J. Nanosci. Nanotechnol.* **2015**, *15*, 9098–9103. [CrossRef]
17. Jang, J.; Son, M.; Chung, S. Low-temperature-grown continuous graphene films from benzene by chemical vapor deposition at ambient pressure. *Sci. Rep.* **2015**, *5*, 17955. [CrossRef]
18. Li, Z.; Ping, W.; Wang, C. Low-Temperature Growth of Graphene by Chemical Vapor Deposition Using Solid and Liquid Carbon Sources. *ACS Nano* **2011**, *5*, 3385–3390. [CrossRef]
19. Choi, J.H.; Li, Z.; Cui, P. Drastic reduction in the growth temperature of graphene on copper via enhanced London dispersion force. *Sci. Rep.* **2013**, *3*, 1925. [CrossRef]
20. Zhao, S.; Luo, Z.; Fang, M.; Wang, Q.; Cen, J. Characteristics of Graphene Growth at Different Temperatures from the Benzene Ring Structure in Coal Tar. *Processes* **2023**, *11*, 593. [CrossRef]
21. Page, A.J.; Wang, Y.; Li, H.B. Nucleation of graphene precursors on transition metal surfaces: Insights from theoretical simulations. *J. Phys. Chem. C* **2013**, *117*, 14858–14864. [CrossRef]
22. Haghighatpanah, S.; Börjesson, A.; Amara, H. Computational studies of graphene growth mechanisms. *Phys. Rev. B* **2012**, *85*, 205448. [CrossRef]
23. Meng, L.J.; Sun, Q.; Wang, J.L. Molecular dynamics simulation of chemical vapor deposition graphene growth on Ni (111) surface. *J. Phys. Chem. C* **2012**, *116*, 6097–6102. [CrossRef]
24. Li, P.; Li, Z.; Yang, J. Dominant Kinetic Pathways of Graphene Growth in Chemical Vapor Deposition: The Role of Hydrogen. *J. Phys. Chem. C* **2017**, *121*, 25949–25955. [CrossRef]
25. Cui, P.; Choi, J.H.; Zeng, C. A Kinetic Pathway toward High-Density Ordered N Doping of Epitaxial Graphene on Cu(111) Using C_5NCl_5 Precursors. *J. Am. Chem. Soc.* **2017**, *139*, 7196–7202. [CrossRef]
26. Tau, O.; Lovergine, N.; Prete, P. Adsorption and decomposition steps on Cu(111) of liquid aromatic hydrocarbon precursors for low-temperature CVD of graphene: A DFT study. *Carbon* **2023**, *206*, 142–149. [CrossRef]
27. Tau, O.; Lovergine, N.; Prete, P. Molecular decomposition reactions and early nucleation in CVD growth of graphene on Cu and Si substrates from toluene. In Proceedings of the SPIE, Low-Dimensional Materials and Devices, San Diego, CA, USA, 18–23 August 2024; Volume 13114, p. 1311409. [CrossRef]
28. Lu, Y.; Yang, X. Molecular simulation of graphene growth by chemical deposition on nickel using polycyclic aromatic hydrocarbons. *Carbon* **2015**, *81*, 564–573. [CrossRef]
29. Ashraf, C.; van Duin, A.C.T. Extension of the ReaxFF Combustion Force Field Towards Syngas Combustion and Initial Oxidation Kinetics. *J. Phys. Chem. A* **2017**, *121*, 1051–1068. [CrossRef]
30. Daw, M.S.; Baskes, M.I. Embedded-atom method: Derivation and application to impurities, surfaces, and other defects in metals. *Phys. Rev. B Condens. Matter* **1984**, *29*, 6443–6453. [CrossRef]
31. Stuart, S.J.; Tutein, A.B.; Harrison, J.A. A reactive potential for hydrocarbons with intermolecular interactions. *J. Chem. Phys.* **2000**, *112*, 6472–6486. [CrossRef]
32. Jones, J.E. On the determination of molecular fields. II. From the equation of state of gas. *Proc. Roy. Soc. A* **1924**, *106*, 463–477. [CrossRef]

33. Li, Z.; Zhang, W.; Fan, X. Graphene Thickness Control via Gas-Phase Dynamics in Chemical Vapor Deposition. *J. Phys. Chem. C* **2012**, *116*, 10557–10562. [CrossRef]
34. Robertson, A.W.; Montanari, B.; He, K. Structural reconstruction of the graphene monovacancy. *ACS Nano* **2013**, *7*, 4495–4502. [CrossRef]